Electronic Supplementary Material (ESI) for Soft Matter.
This journal is © The Royal Society of Chemistry 2020

Supporting Information

for

How clay particulates affect flow cessation and the coiling stability of yield stress-matched cementing suspensions

Iman Mehdipour ([a]), Hakan Atahan ([a],[b]), Narayanan Neithalath ([c]), Mathieu Bauchy ([d],[e]), Edward Garboczi ([f]) and Gaurav Sant ([a],[e],[g],[h],[**])

[a] Laboratory for the Chemistry of Construction Materials (LC^2), Department of Civil and Environmental Engineering, University of California, Los Angeles, CA 90095, USA
[b] Department of Civil Engineering, Istanbul Technical University, Istanbul, Turkey
[c] School of Sustainable Engineering and the Built Environment, Arizona State University, Tempe, AZ, USA
[d] Laboratory for the Physics of Amorphous and Inorganic Solids (PARISlab), Department of Civil and Environmental Engineering, University of California, Los Angeles, CA 90095, USA
[e] Institute for Carbon Management (ICM), University of California, Los Angeles, CA 90095, USA
[f] Applied Chemicals and Materials Division, Material Measurement Laboratory, National Institute of Standards and Technology, Boulder, CO 80305, USA
[g] Department of Materials Science and Engineering, University of California, Los Angeles, CA 90095, USA
[h] California Nanosystems Institute (CNSI), University of California, Los Angeles, CA 90095, USA

[**] Corresponding author: G. Sant, Phone: (310) 206-3084, Email: gsant@ucla.edu

Number of pages: 6 (including the title page)

Number of figures: 9

Number of tables: 0

(A) Coiling speed with air pressure

Figure S1 displays the variations in coiling speed and the resulting gravitational stress rate as a function of pressure of compressed air used in the printer.

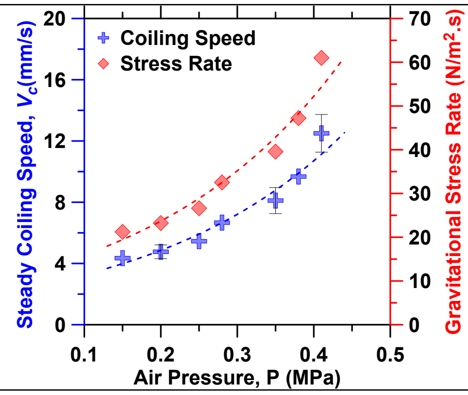

Figure S1: The influence of printer air pressure on coiling speed and resulting gravitational stress rate.

(B) Kinetics of structure formation at varying rest times

The storage modulus evolution of the neat OPC suspension was assessed for varying rest times (see Figure S2a). The pre-shear was set at $\dot{\gamma}$ = 100 s^{-1} for 60 s prior to the rest period. Expectedly, the initial storage modulus of the OPC suspension increased with the rest period. The kinetics of structure development were found, broadly speaking, not to be affected by rest time of 100 s. However, further increasing the rest time to 300 s resulted in somewhat enhanced kinetics of structure formation as noted by the steeper slope of storage modulus evolution. To examine the effect of rest time, the time dependence of overshoot stress for the OPC-clay suspension is shown in Figure S2b.

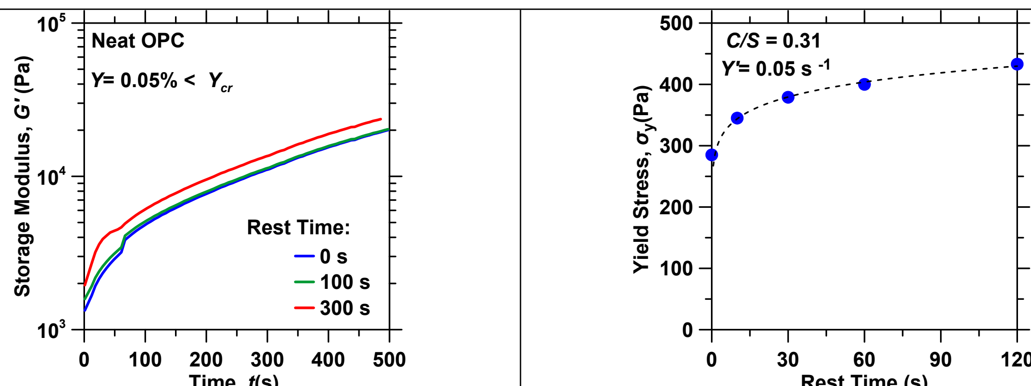

(a)	(b)

Figure S2: (a) The effect of rest time on storage modulus evolution of the neat OPC suspension. **(b)** The time-dependence of stress overshoot of OPC-clay suspension (C/S = 31 %). All measurements were conducted at $\dot{\gamma}$ = 0.05 s^{-1} for varying rest periods, while keeping the pre-shear rate and duration constant. A pre-shear of $\dot{\gamma}$ = 100 s^{-1} for 60 s was carried out. The yield stress shows a tendency to achieve an asymptote with an increasing rest period.

(C) Dynamic light scattering of flocs

The size of flocs as a function of clay dosage is depicted in Figure S3.

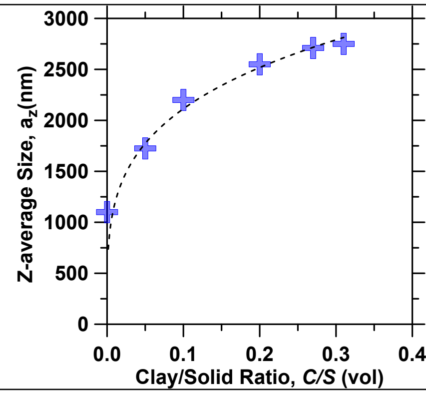

Figure S3: The "Z-average" size of aggregates as determined by dynamic light scattering (DLS) in OPC-clay suspensions (0.05 $g_{solid}/L_{solution}$). These values are indicative of floc size.

(D) Rheological properties with particle volume fraction

The effects of particle volume fraction on yield stress and relative viscosity as a function of clay dosage are displayed in Figure S4.

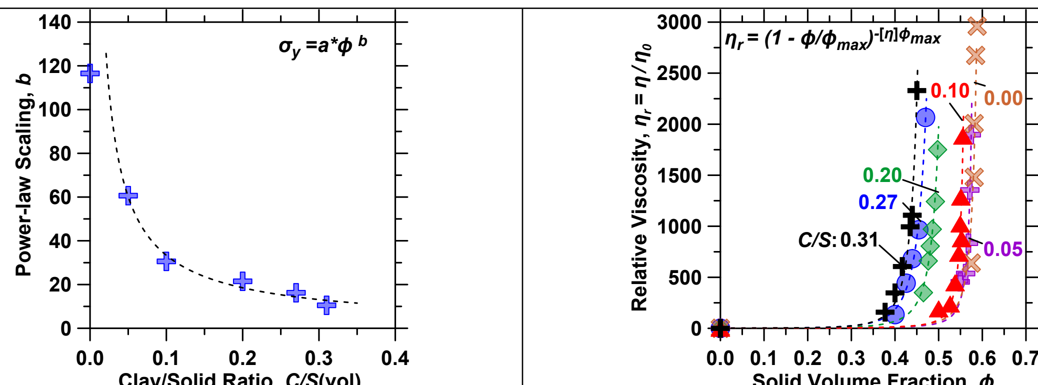

(a)	(b)

Figure S4: (a) The power-law scaling behavior *b* of the yield stress of suspensions across varying clay dosages. Scaling *b* was obtained by fitting a power-law function of the form $\sigma_y = a(\phi)^b$ to yield stress-particle volume fraction curves. **(b)** The relative viscosity of the suspensions in relation to solid volume fraction for varying clay dosages. The data were fitted by the Krieger–Dougherty equation. The relative viscosity was determined as ratio viscosity of suspension to the viscosity of the continuous phase (i.e., water).

(E) Interparticle interaction potential between clay particles in OPC-clay suspensions

The interparticle interaction potential (V) between clay particles as a function of distance from the particle surface in two different aqueous solutions (DI water and cement pore solution) were assessed (see Figure S5). The calculated interparticle potential (Equation S1) includes the contributions of electrostatic repulsion (V_{es}) that was modeled using the Hogg-Healy-

Fuerstenau[1] solution to the Poisson-Boltzmann equation, and van der Waals attraction (V_{vdW}), calculated using the nonretarded Hamaker pair potentials.[2,3]

$$V(x) = V_{es}(x) + V_{vdW}(x) = \pi \varepsilon_r \varepsilon_0 \psi^2 R \ln\left[1 + \exp\left(-\kappa x\right)\right] - \frac{AR}{12x} \qquad \textbf{Equation S1}$$

Here, ε_r and ε_0 are the relative permittivity and permittivity of free space, respectively, and R is particle radius. The characteristic electrostatic decay length, or Debye length κ^{-1} was estimated as $\kappa^{-1} = \sqrt{\varepsilon_r \varepsilon_0 kT/2e^2 I}$, with k, T and e being the Boltzmann constant, temperature, and the elementary charge, respectively, and I being the ionic strength of the medium defined as $0.5\sum c_i z_i^2$ with c_i and z_i being the molar concentration and the valence of each ionic species present in the solution.

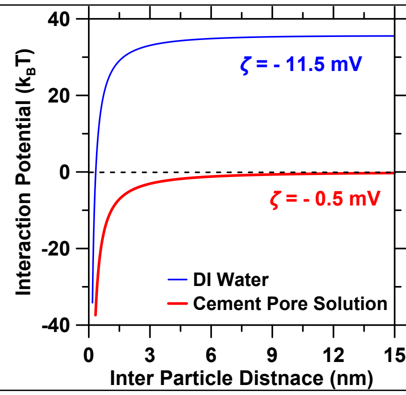

Figure S5: The calculated interparticle potentials based on electrostatic and van der Waals interactions for clay particulates suspended in either DI water or cement pore solution (i.e., saturated cement solution; pH 12.5).

(F) Rheological hysteresis

The rheological hysteresis loop data was complied for the plain OPC suspension and OPC-clay suspension (C/S = 31 %). Herein, the hysteresis loop was generated by recording reversal flow curves starting by downward shear rate sweep followed by upward sweep. The plain OPC suspension exhibited divergence in shear stress during downward shear rate sweep, while this behavior was substantially suppressed for the OPC-clay suspension (see Figure S6). Furthermore, on account of higher thixotropic structure rebuilding, the OPC-clay suspension featured a greater hysteresis loop area than that of the plain OPC suspension.

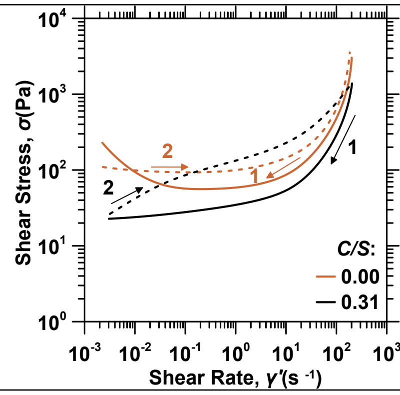

Figure S6: Rheological hysteresis loops of OPC-clay suspensions during downward flow sweep (1) followed by upward flow sweep (2).

(G) Shear thickening/thinning behavior

The viscosity as a function of shear rate for the OPC-clay suspensions composed at varying clay dosages is depicted in Figure S7. The discontinuous shear thickening transition was only noted for the neat OPC suspension while suspensions loaded with clay exhibited only shear thinning behavior over the range of the shear rate sweep.

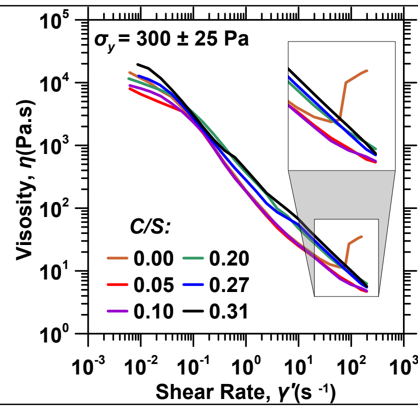

Figure S7: The viscosity as a function of the shear rate for OPC-clay suspensions composed at varying clay dosages.

(H) Strain-retardation time

Although the retardation times were extracted by fitting a Kelvin–Voigt model of the form

$$\gamma_t = \sum_{i=1}^{N=10} A_i\left(1 - e^{-t/t_{r,i}}\right)$$

to each shear stress cycle, in effect, strain did not truly reach a plateau, specially at higher shear stress cycles, as indicated in the zoomed view (Figure S8).

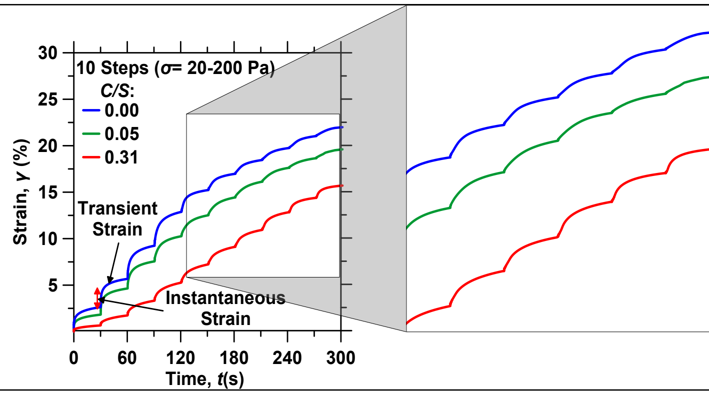

Figure S8: The zoomed view of the evolution of strain with stepwise changes in shear stress for varying clay dosages. The zoomed view indicates that strain did not truly reach a plateau, especially at higher shear stress cycles.

(I) Viscoelastic properties

The storage modulus trends as a function of amplitude sweep and the evolution of the storage modulus of OPC-clay suspensions are displayed in Figure S9. Double yielding was only noted for the neat cement (OPC) suspension, while the clay-containing suspensions exhibited a single yielding point. This transition from double to single yielding point results from the strong interparticle interactions between clay/clay and clay/OPC particles in the OPC-clay suspensions.

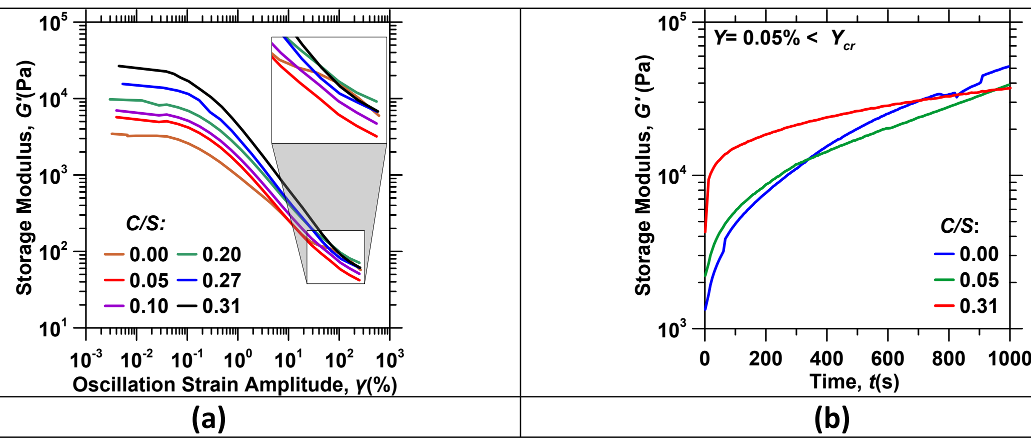

Figure S9: **(a)** The storage modulus as a function of oscillation strain of dense suspensions for varying clay dosages. **(b)** The time-dependent storage modulus evolution of OPC-clay suspensions.

References

1 R. Hogg, T. W. Healy and D. W. Fuerstenau, *Trans. Faraday Soc.*, 1966, **62**, 1638–1651.
2 H. C. Hamaker, *Physica*, 1937, **4**, 1058–1072.
3 U. Aschauer, O. Burgos-Montes, R. Moreno and P. Bowen, *J. Dispers. Sci. Technol.*, 2011, **32**, 470–479.